AN EXCITED STATE PHOTOELECTROCHEMICAL CELL FOR THE PRODUCTION OF H_2O_2 AND Br_2

JOSEPH P. OTRUBA, GREGORY A. NEYHART, WALTER J. DRESSICK, JANET L. MARSHALL, B. PATRICK SULLIVAN, PENNY A. WATKINS and THOMAS J. MEYER

Chemistry Department, The University of North Carolina, Chapel Hill, NC 27514 (U.S.A.)

(Received March 3, 1986)

Summary

The design and operation of a series of oxidative excited state photoelectrochemical half-cells is described, as is the application of one of them to the production of H_2O_2 and Br_2 in separate cell compartments in acetonitrile solution. The basis for the half-cells is in the series of steps: (1) optical excitation of the metal-to-ligand charge transfer chromophore in complexes such as $(bpy)Os(das)_2^{2+}$ (bpy is 2,2′-bipyridine; das is 1,2-bis-dimethylarsinobenzene), (2) reductive quenching of the excited states by $N(p\text{-}C_6H_4Br)_3$ (NAr_3), (3) scavenging of the reduced metal complex in acidic acetonitrile by O_2 which gives H_2O_2 and builds up NAr_3^+ and (4) transfer of the oxidizing equivalents in NAr_3^+ through an external circuit to a dark anode compartment where oxidation occurs. In the H_2O_2/Br_2 cell, Br^- is oxidized to Br_2 in the second compartment. A kinetic model developed earlier has been successfully applied to the $(bpy)Os(das)_2^{2+}$ half-cell; this successfully predicts variations in photocharge with variations in chromophore, quencher and O_2 concentrations, incident light intensity and added acid. In an air-saturated solution saturated with quencher the cell efficiency for the production of H_2O_2 and Br_2 at high limiting concentrations of quencher is $\phi'_{cell} = 0.85 \pm 0.05$ (equivalents of photoproducts per photon absorbed) at 25 °C. Under the same air-saturated conditions, the most efficient half-cell is based on the chromophore $Ru(4,4'\text{-}(CO_2Et)_2bpy)_3^{2+}$ ($4,4'\text{-}(CO_2Et)_2bpy$ is 4,4′-bis(carboethoxy)-2,2′-bipyridine) where $\phi'_{cell} = 1.8 \pm 0.05$. ϕ_{cell} values in excess of unity provide evidence for a kinetic step in which the one-electron intermediate HO_2 is reduced by NAr_3 to give a second mole of NAr_3^+ per photon absorbed.

1. Introduction

A commonly explored strategy for energy conversion processes based on molecular excited states involves optical excitation and subsequent quenching of the resulting excited state or states by electron transfer [1 - 5].

0047-2670/86/$3.50

Metal-to-ligand charge transfer (MLCT) excited states of transition metal complexes such as $Ru(bpy)_3^{2+}$ (bpy is 2,2′-bipyridine) have been especially popular in such studies. Their excited states can be quenched either oxidatively or reductively in well-defined reactions, *e.g.*

$$Ru(bpy)_3^{2+} \xrightarrow{h\nu} Ru(bpy)_3^{2+*} \quad (1)$$

$$Ru(bpy)_3^{2+*} + PQ^{2+} \longrightarrow Ru(bpy)_3^{3+} + PQ^{+} \quad (2)$$

(PQ^{2+} is Me—$^{+}$N⬡—⬡N^{+}—Me)

$$Ru(bpy)_3^{2+*} + TMBD \longrightarrow Ru(bpy)_3^{+} + TMBD^{+} \quad (3)$$

(TMBD is Me_2N—⬡—⬡—NMe_2)

However, the redox energy stored following excitation and quenching is stored only transiently because of recombination, via back electron transfer, *e.g.*

$$Ru(bpy)_3^{3+} + PQ^{+} \longrightarrow Ru(bpy)_3^{2+} + PQ^{2+} \quad (4)$$

$$Ru(bpy)_3^{+} + TMBD^{+} \longrightarrow Ru(bpy)_3^{2+} + TMBD \quad (5)$$

One approach to the problem of converting light energy to chemical energy is the excited state photoelectrochemical cell [5 - 10]. Such cells, as they have been operated thus far, consist of two half-cell compartments connected by both a salt bridge and an external electrical circuit. The excitation and quenching acts take place in one of the two half-cell compartments. In the presence of a scavenger for one of the quenching products, *e.g.* triethanolamine or H_2EDTA^{2-} (EDTA is ethylenediaminetetraacetate) for $Ru(bpy)_3^{3+}$ produced in eqn. (2), photoredox equivalents in the form of PQ^{+} build up during photolysis, and can be used to reduce protons in the second cell compartment [11] as in

$$H^{+} \xrightarrow[Pt]{+e^{-}} \frac{1}{2} H_2 \quad (6)$$

The electrode compartment photolyzed in such a cell acts as a photoanode compartment for the oxidation of the scavenger.

We describe here the design and operation of a series of oxidative excited state photoelectrochemical half-cells and the application of one of them to the production of H_2O_2 and Br_2 in separate cell compartments with high per photon absorbed quantum efficiencies [12]. The distinctive feature of the cells is that, although they do rely on a scavenger for their operation, the scavenger is O_2 and it leads ultimately to H_2O_2 via the net reaction

$$O_2 + 2H^{+} + 2Br^{-} + h\nu \longrightarrow H_2O_2 + Br_2 \quad (7)$$

2. Experimental details

2.1. Materials

Acetonitrile (Burdick and Jackson), perchloric acid (Baker, 70%), lithium perchlorate (G. Frederick Smith), hydrogen peroxide (Baker, 30%), tetra(*n*-butyl)ammonium bromide (Aldrich) and N_2–O_2 mixtures (Matheson) were all reagent grade and used without further purification. *N,N,N',N'*-tetramethylbenzidine (Aldrich) was purified twice by sublimation.

2.2. Syntheses

2.2.1. Tris(4-bromophenyl)amine

The amine was synthesized using the method of Baker *et al.* [13] and was recrystallized twice from methanol: yield, 78%; melting point, 144 - 145 °C (144.5 - 146.5 °C is given in ref. 13); nuclear magnetic resonance (60 Hz, CD_3CN), δ = 6.95 (doublet), δ = 7.3 (doublet).

2.2.2. [(bpy)Os(das)$_2$](PF$_6$)$_2$ (bpy is 2,2'-bipyridine; das is 1,2-bis-(dimethylarsino)benzene)

[(bpy)Os(das)$_2$](PF$_6$)$_2$, which was first synthesized by Caspar [14] was prepared by heating (bpy)$OsCl_4$ (0.16 g, 0.31 mmol) [15] and das (0.67 g, 2.3 mmol, Strem Chemicals) in 30 ml ethylene glycol (Fisher certified grade) at reflux for 16 h under argon. The complex was precipitated by adding a solution of 1 g NH_4PF_6 (Aldrich) in 60 ml distilled H_2O, and purified by column chromatography on alumina with acetonitrile–toluene mixtures used as eluant. The yield is 79%.

2.2.3. [(phen)Os(das)$_2$](PF$_6$)$_2$ (phen is 1,10-phenanthroline)

[(phen)Os(das)$_2$](PF$_6$)$_2$ was synthesized in a manner analogous to (bpy)Os(das)$_2^{2+}$, with (phen)$OsCl_4$ used as a starting material.

2.2.4. [Ru(bpyz)$_3$](PF$_6$)$_2$ and [Ru(bpym)$_3$](PF$_6$)$_2$ (bpyz is 2,2'-bipyrazine and bpym is 2,2'-bipyrimidine)

[Ru(bpyz)$_3$](PF$_6$)$_2$ and [Ru(bpym)$_3$](PF$_6$)$_2$ were prepared using the method of Rillema *et al.* [16].

2.2.5. [Ru(4,4'-(CO$_2$Et)$_2$-2,2'-bpy)$_3$](PF$_6$)$_2$ (4,4'-(CO$_2$Et)$_2$-2,2'-bpy is 4,4'-bis(carboethoxy)-2,2'-bipyridine)

[Ru(4,4'-(CO$_2$Et)$_2$-2,2'-bpy)$_3$](PF$_6$)$_2$ was prepared using the method of DeLaive *et al.* [17].

2.2.6. [(bpy)$_2$Ru(PPh$_3$)Cl](PF$_6$)

[(bpy)$_2$Ru(PPh$_3$)Cl](PF$_6$) was prepared using the method of Sullivan *et al.* [18].

2.3. Measurements

UV–visible spectra were obtained using Bausch and Lomb 2000 or Varian 634 spectrophotometers. Photolyses were carried out using radiation

from a Hanovia 977B0010 1000 W high pressure Hg–Xe arc lamp in an LH151N Schoeffel lamp housing. The light was passed through a Bausch and Lomb high intensity monochromator (33-66-79) to select out the 436 nm line. Photocurrents were monitored on a Hewlett Packard $X-Y$ recorder using a 1000 Ω resistor. Integration of the current–time plots gave the photocharge. Quantum yields are based on ferrioxalate actinometry [19]. Lifetime measurements were obtained as described earlier [20]. Reported potentials are measured against the saturated sodium calomel electrode (SSCE). Analyses were performed by Galbraith Laboratories, Knoxville, TN.

2.4. Cell design

A three-compartment cell was used, as shown in Fig. 1. The photocathode was a quartz cuvette 1 cm square containing a platinum gauze electrode affixed to one window. The photocathode compartment was equipped with a magnetic stirrer. The three compartments were separated by glass frits with the center compartment containing only electrolyte. The anode compartment, which was not stirred, was also equipped with a platinum gauze electrode.

2.5. Experimental conditions

In all cases, the solvent was acetonitrile and the electrolyte was 0.10 M $LiClO_4$. In a typical run, the photocathode compartment contained 5×10^{-5} M $[(bpy)Os(das)_2](PF_6)_2$ (optical density $OD_{436\,nm} = 0.090$), 7×10^{-3} M of

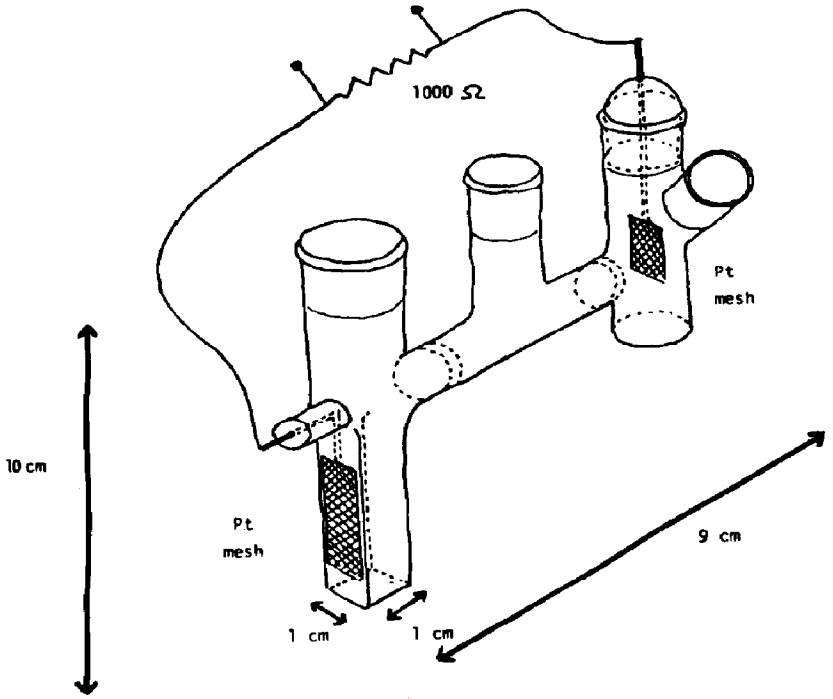

Fig. 1. Three-compartment cell used for photolyses.

the quencher tris(4-bromophenyl)amine (NAr_3) and 0.30 M $HClO_4$. For quantum yield measurements, the anode contained 10^{-2} M *N,N,N',N'*-tetramethylbenzidine (TMBD) which was easier to use than the $[(bpy)_2Ru(PPh_3)Cl]^+/Br^-$ system described below, since the product, $TMBD^+$, is highly colored ($\lambda_{sh,790\,nm} = 5.62 \times 10^3\ M^{-1}\ cm^{-1}$) and easily analyzed spectrophotometrically. The cell was not degassed. The photocathode compartment was irradiated at 436 nm ($I_0 = 5.6 \times 10^{-9}$ einsteins s^{-1}) and the current monitored using a 1000 Ω resistor and a chart recorder. The total charge passed was obtained by integrating current–time plots. As a check, the amount of $TMBD^+$ produced was measured spectrophotometrically and shown to agree with the number of electrons passed to within 10%.

2.6. Analysis of bromine

In a solution 0.1 M in $[(n\text{-}Bu)_4N](PF_6)$ in acetonitrile, a cyclic voltammogram shows a quasi-reversible wave at $E_{p,anodic} = +0.73$ V(SSCE) for the Br^-/Br_3^- couple; Br_2 produced at the electrode is rapidly converted to Br_3^- in the presence of excess Br^- [21]. The oxidative component is relatively sharp, but the return reductive wave is broad and ill defined. A second quasi-reversible wave appears at $E_{1/2} = +0.95$ V(SSCE) ($\Delta E_p = 140$ mV) which probably has its origin in the Br_3^-/Br_2 couple [21].

Photoelectrochemical experiments in the presence or absence of the electron transfer catalyst $[(bpy)_2Ru(PPh_3)Cl]^+$ ($E_{1/2}(Ru^{III}/Ru^{II}) = 0.94$ V) [18] where the oxidation of Br^- is indirect

$$2(bpy)_2Ru^{II}(PPh_3)Cl^+ \xrightarrow[Pt]{-2e^-} 2(bpy)_2Ru^{III}(PPh_3)Cl^{2+} \quad (8)$$

$$2(bpy)_2Ru^{III}(PPh_3)Cl^{2+} + 2Br^- \longrightarrow 2(bpy)_2Ru^{II}(PPh_3)Cl^+ + Br_2 \quad (9)$$

gave the same results.

The concentration of Br_2 (or Br_3^-) produced in the photolysis was determined by an indirect spectrophotometric method in which an excess of TMBD was added. The $TMBD^+$ produced

$$TMBD + \frac{1}{2}Br_2 \longrightarrow TMBD^+ + Br^- \quad (10)$$

was then determined spectrophotometrically at 790 nm. A separate series of spectrophotometric experiments showed that eqn. (10) is quantitative as written, at least for TMBD in excess.

2.7. [H_2O_2] analysis

The analysis of H_2O_2 was based on the enzyme method of Mottola *et al.* [22] involving the peroxidase-catalyzed oxidation of leuco crystal violet with subsequent measurement of the absorbance due to the crystal violet cation dye at 594 nm. This method was chosen because of its sensitivity (1.75×10^{-6} M H_2O_2 detection limit) and the fact that the wavelength for analysis is separated from the operating wavelength of the cell. After

the photocurrent had been allowed to return to zero following an irradiation period exceeding 60 min, a 1 ml aliquot was added to a solution containing 4 ml of (2 M sodium acetate)–(2 M acetic acid) and 1 ml of a 1.29×10^{-3} M leuco crystal violet solution in 0.5% HCl–H_2O. This was followed immediately by the addition of aqueous peroxidase enzyme solution (activity of 12.95 units per millilitre). The resulting solution was diluted to 10 ml with conductivity water and centrifuged for 5 min at 90 000 rev min^{-1} to remove the fine suspension of $N(p\text{-}C_6H_4Br)_3$ which forms on addition of H_2O to the CH_3CN cell solution. Absorbance of the solution at 594 nm was measured and the H_2O_2 concentration was determined from a prepared calibration curve. All manipulations were carried out in the dark to prevent further production of H_2O_2 and/or $N(p\text{-}C_6H_4Br)_3^+$, both of which can oxidize leuco crystal violet. The calibration curve was derived from H_2O_2 standard solutions. These solutions were prepared in the dark by dilution of a stock 30 vol.% aqueous H_2O_2 solution (Fisher) with 0.1 M $LiClO_4$–CH_3CN containing the appropriate amounts of metal complex, quencher and acid to give levels identical with those used in the cell experiments. The 30 vol.% H_2O_2 solution was standardized immediately before use with 0.100 N $KMnO_4$, whose concentration was determined prior to use with the primary standard sodium oxalate.

3. Results and discussion

3.1. Design of the cells

The design of the cells was based on earlier work where it had been shown that following reductive quenching of $Ru(bpy)_3^{2+*}$ by dimethylaniline (DMA) in air-saturated acetonitrile solution

$$Ru(bpy)_3^{2+*} + DMA \longrightarrow Ru(bpy)_3^{+} + DMA^{+} \quad (11)$$

$Ru(bpy)_3^{+}$ could be scavenged by O_2 giving O_2^-

$$Ru(bpy)_3^{+} + O_2 \longrightarrow Ru(bpy)_3^{2+} + O_2^- \quad (12)$$

The subsequent electron transfer between DMA^+ and O_2^-

$$DMA^{+} + O_2^- \longrightarrow DMA + O_2 \quad (13)$$

was followed by conventional flash photolysis [23].

In acidic aqueous solution O_2^- is protonated to give the perhydroxyl radical ($pK_a(HO_2) = 4.69 \pm 0.08$) [24] which is unstable with respect to disproportionation into H_2O_2 and O_2

$$2HO_2 \longrightarrow H_2O_2 + O_2 \quad (14)$$

($k(23\ ^\circ C) = (8.60 \pm 0.62) \times 10^5\ M^{-1}\ s^{-1}$) [24].

Our thought was that in acetonitrile solution with added acid the sequence of reactions (11), (12) and (14) should lead to the photoproduction of H_2O_2 and the oxidized form of the quencher using visible light

$$\frac{1}{2}O_2 + H^+ + DMA + h\nu \longrightarrow DMA^+ + \frac{1}{2}H_2O_2 \quad (15)$$

In an electrochemical cell arrangement the sequence of reactions opens the possibility of a general device for carrying out oxidations in a second cell compartment based on the oxidizing equivalents stored as DMA^+.

However, the $DMA^{+/0}$ couple is not very strongly oxidizing ($E^{0\prime}$ = +0.85 V(SSCE)) and the DMA^+ cation is unstable even for short periods in solution. In order to overcome these limitations we have turned to more strongly oxidizing excited states which have allowed us to use the $N(p\text{-}C_6H_4Br)_3^{+/0}$ couple ($NAr_3^{+/0}$) which is more strongly oxidizing ($E^{0\prime}$ = +1.07 V(SSCE) in CH_3CN) and whose radical cation is stable for extended periods in acetonitrile solution. Given the relatively high formal potential for the $NAr_3^{+/0}$ couple, an attractive reaction for the anode compartment is oxidation of Br^- to Br_2/Br_3^-. Br_2 is a useful chemical oxidant and, from electrochemical measurements in CH_3CN, the driving force is relatively low for the net reaction (about 0.4 V)

$$2NAr_3^+ + 3Br^- \longrightarrow 2NAr_3 + Br_3^- \quad (16)$$

meaning that the oxidizing strength of NAr_3^+ is transferred in relatively high efficiency to the chemical product.

3.2. Oxidative photoelectrochemical half-cells

In Table 1 are summarized the excited state properties (emission energy, lifetime and reduction potential) of relevance for the series used here

TABLE 1

Excited state properties and ϕ'_{cell} values in CH_3CN [a]

Complex	E_{em} [b] ($\times 10^{-3}$ cm^{-1})	$E^{0\prime}(M^{2+/+})$ [c] (V)	$E^{0\prime}(M^{2+*/+})$ [d] (V)	τ [e] (ns)	ϕ'_{cell} [f]
$(bpy)Os(das)_2^{2+}$	16.9	−1.0	1.14	555	0.85
$(phen)Os(das)_2^{2+}$	16.9	−1.0	1.14	390	0.90
$Ru(bpyz)_3^{2+}$	16.4	−0.68	1.40	555	0.05
$Ru(bpym)_3^{2+}$	15.8	−0.91	1.14	94	0.30
$Ru(4,4'\text{-}(CO_2Et)_2bpy)_3^{2+}$	15.5	−0.69	1.23	567	1.8

[a] Photolysis time, 1000 s; T = 295 K; $A_{436\,nm;\,M^{II}} = 0.090$; $[NAr_3] = 7 \times 10^{-3}$ M; $I^0 = 5.6 \times 10^{-9}$ einsteins s^{-1}; air saturated.

[b] Corrected emission energy in CH_3CN at λ^{em}_{max}.

[c] Reduction potential for the first polypyridyl-based ground state couple, *e.g.* $(bpy)Os^{II}(das)_2^{2+}/(b\bar{p}y)Os^{II}(das)_2^{+}$ measured against an SSCE.

[d] Reduction potential for the metal-based excited state couple, *e.g.* $(b\bar{p}y)Os^{III}(das)_2^{2+*}/(b\bar{p}y)Os^{II}(das)_2^{+}$ measured against an SSCE. Calculated from $E^{0\prime}(M^{2+*/+}) = E_{em} + E^{0\prime}(M^{2+/+})$.

[e] Excited state lifetimes in air-saturated CH_3CN.

[f] Equivalents of photocharge produced per photon absorbed in a solution saturated in quencher as described in footnote a.

as a basis for oxidative photoelectrochemical half-cells. An important property is the ability of the excited state to act as an oxidizing agent toward the quencher, *e.g.*

$$(bpy)Os(das)_2^{2+*} + NAr_3 \longrightarrow (bpy)Os(das)_2^{+} + NAr_3^{+} \quad (17)$$

$$E^{0\prime}(M^{2+*/+}) = +1.14 \text{ V}$$

The ligand abbreviations used in Table 1 and elsewhere are bpy for 2,2′-bipyridine, phen for 1,10-phenanthroline, das for 1,2-bis(dimethylarsino)-benzene, bpyz for 2,2′-bipyrazine, bpym for 2,2′-bipyrimidine and 4,4′-$(CO_2Et)_2$bpy for 4,4′-bis(carboethoxy)-2,2′-bipyridine; the structures for the last four are shown below:

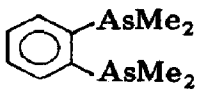

das

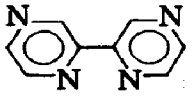

bpyz

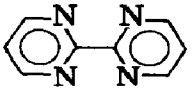

bpym

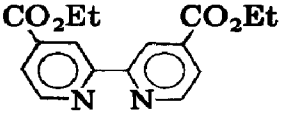

4, 4′-$(CO_2Et)_2$bpy

A series of photoelectrochemical half-cells based on the excited states listed in Table 1 has been investigated. In one type of experiment the per photon absorbed quantum yield for the production of NAr_3^+ was measured for the series of chromophores. The conditions were air-saturated CH_3CN, 0.30 M $HClO_4$, $[NAr_3] = 7 \times 10^{-3}$ M (saturated), $I^0(436 \text{ nm}) = 5.6 \times 10^{-9}$ einsteins s^{-1} (I^0 is the incident light intensity), $T = 295$ K and a photolysis time of 1000 s. The actual measurement made was of the photocurrent produced by the indirect oxidation of *N,N,N′,N′*-tetramethylbenzidine (TMBD) in the anode compartment:

$$TMBD \xrightarrow{-e^-} TMBD^+ \quad (18)$$

In Fig. 2 is shown the photocurrent–time profile obtained in such an experiment based on $(bpy)Os(das)_2^{2+}$ as the chromophore and using the cell design shown in Fig. 1. Equations have been derived for related excited state photoelectrochemical cells which describe the photocurrent response and integrated photocharge in terms of the properties of the cells [11, 25]. From that work, the photocharge q_p, obtained by integration of the current–time curve, is related to the incident light intensity I^0 (einsteins s^{-1}), the per photon absorbed cell efficiency ϕ'_{cell} and the photolysis time t (s) by

$$q_p = nFI^0(1 - 10^{-A_{Os}}) \frac{A_{Os}}{A_{Os} + A_{NAr_3^+}} \phi'_{cell} t \quad (19)$$

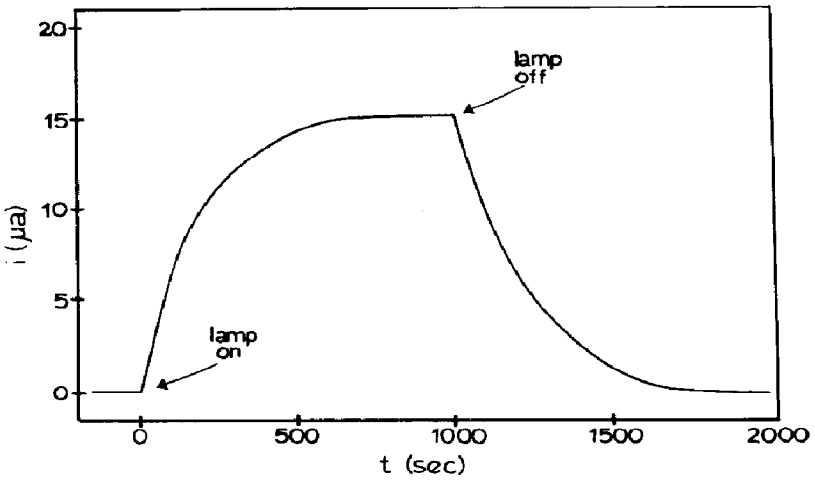

Fig. 2. Typical current–time response of an excited state photoelectrochemical cell during photolysis under typical conditions: $[(bpy)Os(das)_2^{2+}] = 5 \times 10^{-5}$ M; $[NAr_3] = 7 \times 10^{-3}$ M; $[HClO_4] = 0.30$ M; $I^0(436\ nm) = 5.6 \times 10^{-9}$ einsteins s^{-1}; $T = 295$ K; $t = 1000$ s; air-saturated solution.

In eqn. (19), ϕ'_{cell} is the per photon absorbed quantum efficiency at a fixed concentration (saturated solution) of quencher. $n = 1$ is the number of electrons transferred in the electrode reaction, F is the Faraday constant (96 484 C mol^{-1}) and A_{Os} and $A_{NAr_3^+}$ are the absorbances of the chromophore and the oxidized form of the quencher at the photolysis wavelength (436 nm). Equation (19) is valid only if all the incident light enters the solution and if effects arising from reflection from the electrode are neglected.

The quencher is transparent at 436 nm but NAr_3^+ is not ($\epsilon(436\ nm) = 270\ M^{-1}\ cm^{-1}$) and if it builds up during the photolysis it could become a significant competitive light absorber. In order to avoid such complications, the sensitizer concentrations were held relatively low with $A_{436} \approx 0.10$ in order to avoid the build-up of NAr_3^+.

Per photon absorbed quantum efficiencies in solutions saturated in quencher ϕ'_{cell} were determined using eqn. (19) and q_p values obtained by integration of current–time curves similar to that shown in Fig. 2. Values of ϕ'_{cell} obtained by measuring the $TMBD^+$ produced in the anode ($\epsilon(790\ nm) = 5620\ M^{-1}\ cm^{-1}$) were within experimental error of the values obtained by photocharge measurements.

Values of ϕ'_{cell} obtained in solutions saturated in quencher are summarized in Table 1. Interestingly, the data show a considerable variation in ϕ'_{cell} with chromophore and, further, in the best case, using $Ru(4,4'-(CO_2Et)_2bpy)_3^{2+}$ as chromophore, ϕ'_{cell} can actually exceed unity. The advantages of the ruthenium complex as chromophore, at least compared with $(bpy)Os(das)_2^{2+}$, are clearly illustrated in the absorption spectra in Fig. 3. The variations in ϕ'_{cell} with chromophore are reconcilable based on the photoelectrochemical mechanism proposed in Fig. 6 below.

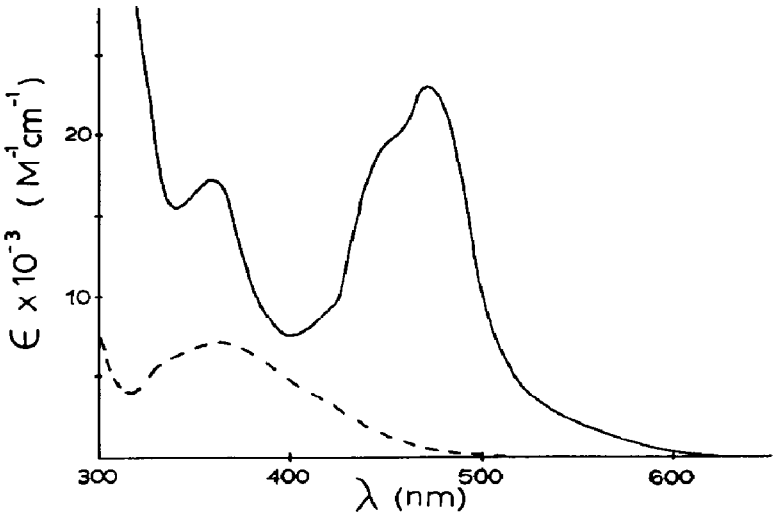

Fig. 3. Absorption spectra of $(bpy)Os(das)_2^{2+}$ (———) and $Ru(4,4'\text{-}(CO_2Et)_2bpy)_3^{2+}$ (——).

3.3. Photoelectrochemical production of H_2O_2 and Br_2

In a second type of experiment, a photoelectrochemical cell was set up for the production of Br_2. The cell utilized $(bpy)Os(das)_2^{2+}$ as the chromophore and the same experimental conditions described in Fig. 2. The concentrations of H_2O_2 in the photocathode compartment and of Br_2/Br_3^- in the anode compartment were determined as described in Section 2 and ϕ'_{cell} as described above. The per photon absorbed quantum yields obtained for the three measured quantities were $\phi'_{H_2O_2} = 0.35 \pm 0.10$, $\phi'_{Br_2} = 0.37 \pm 0.04$ and $\phi'_{cell} = 0.85 \pm 0.05$. Since ϕ'_{cell} is based on photocharge measurements, the relationship between the three quantities is predicted to be $\phi'_{H_2O_2} = \phi'_{Br_2} = \frac{1}{2}\phi'_{cell}$. The experimental relationships are sufficiently close to verify that the overall reaction in the cell is

$$O_2 + 2H^+ + 2Br^- \xrightarrow{h\nu} H_2O_2 + Br_2 \qquad (7)$$

with Br_3^- the net product in the presence of excess Br^-.

The cell based on $(bpy)Os(das)_2^{2+}$ was also used to verify the linear dependence on incident light intensity predicted by eqn. (19). In Fig. 4 is shown a plot of q_p *versus* I^0 under a constant set of conditions except that the light intensity was varied. The linear relationship is significant in that it demonstrates that the initiating photochemical event is monophotonic.

When the cell reaches its photostationary state, the photocurrent reaches a plateau as shown in Fig. 2. Under these conditions the osmium complex exists largely as osmium(II) because of rapid capture of osmium(I) by O_2 and the low light intensities used. However, NAr_3^+ is a photoproduct. Its diffusion to the electrode and subsequent electroreduction provide the basis for the photocurrent in the cell. From the current–time profile in

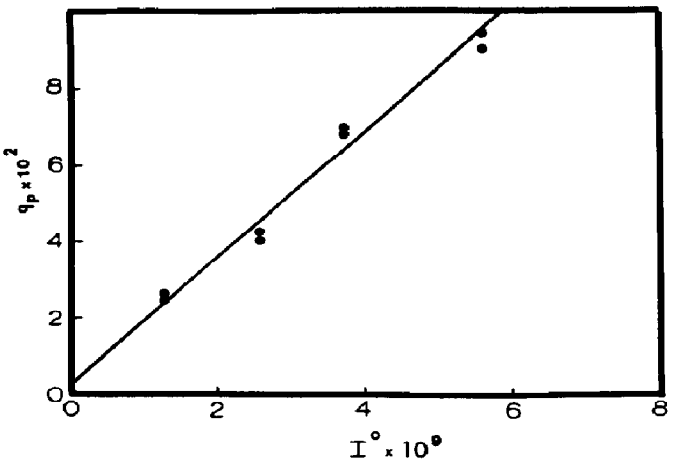

Fig. 4. Plot of q_p (C) *vs.* I^0 (einsteins s^{-1}) under conditions where $[(bpy)Os(das)_2^{2+}] = 5 \times 10^{-5}$ M, $[NAr_3] = 7 \times 10^{-3}$ M, $[HClO_4] = 0.30$ M, $T = 295$ K, $t = 1000$ s and the solution is air saturated (slope, 160 ± 20 C s einstein^{-1}; intercept, 26 ± 60 C; correlation coefficient, 0.993).

Fig. 2, $[NAr_3^+]$ increases with time initially and finally reaches a steady state. At the steady state, the rate of diffusion to and reduction of NAr_3^+ at the electrode reaches its rate of photochemical production.

It is possible to use the absorbance term in eqn. (19) to estimate $[NAr_3^+]$ at the steady state. As the concentration of chromophore is increased, the concentration of NAr_3^+ at the steady state increases. If light absorption by NAr_3^+ becomes appreciable, the fraction $A_{Os}/(A_{Os} + A_{NAr_3^+})$ should fall below unity and affect the operation of the cell.

In Fig. 5 is shown a plot of q_p *versus* $1 - 10^{-A_{Os}}$ and an extrapolation of the plot to high concentrations of chromophore on the assumption that $A_{Os}/(A_{Os} + A_{NAr_3^+}) = 1$. At high concentrations of chromophore there is clear evidence of deviation from Beer's law behavior because of light absorption by NAr_3^+. On the basis of the extent of the deviation, it is possible to calculate a lower limit on the concentration of NAr_3^+ at the steady state as a function of chromophore concentration using

$$[NAr_3^+] \leqslant \frac{A_{Os}(436\text{ nm})}{b\epsilon_{NAr_3^+}(436\text{ nm})}\left(\frac{q_{p,\text{extrap}}}{q_{p,\text{exptl}}} - 1\right) \qquad (20)$$

Equation (20) gives only a lower limit for $[NAr_3^+]$ at the steady state because it includes contributions from early in the photolysis period before $[NAr_3^+]$ reaches the steady state level. In eqn. (20) $q_{p,\text{extrap}}$ and $q_{p,\text{exptl}}$ are the extrapolated and experimental values in Fig. 5, $\epsilon_{NAr_3^+}(436\text{ nm}) = 270$ M^{-1} cm^{-1} and the cell path length b is 1 cm. On the basis of the data in Fig. 5, at the steady state $[NAr_3^+] \leqslant 4.1 \times 10^{-5}$ M, 4.2×10^{-4} M and 1.4×10^{-3} M at $[(bpy)Os(das)_2^{2+}]$ equal to 1.0×10^{-4} M, 2.2×10^{-4} M and 4.2×10^{-4} M respectively.

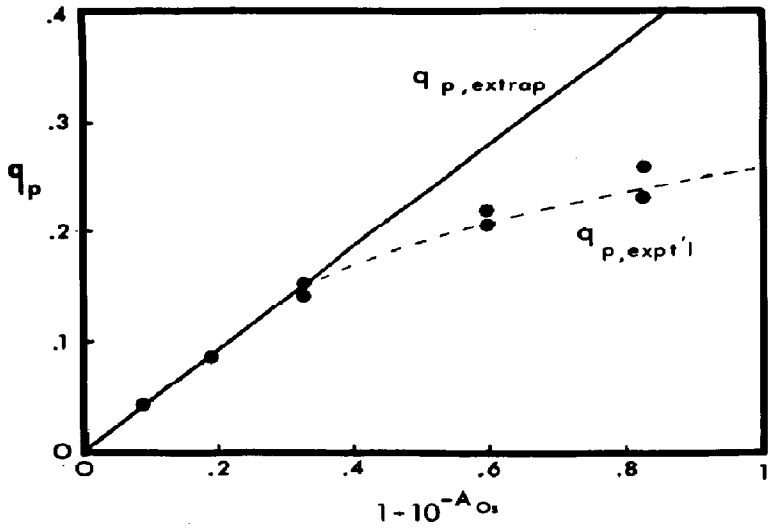

Fig. 5. Plot of q_p (C) *vs.* $1 - 10^{-A}$Os using the same conditions as in Fig. 4 except with varying amounts of $[(bpy)Os(das)_2^{2+}]$. The plot shows the deviation from simple Beer's law behavior at high chromophore concentrations: ——, extrapolated line with slope of 0.47 C; — — —, experimental curve.

3.4. Photoelectrochemical mechanism

A series of experiments was carried out with the aim of analyzing in more detail the individual steps that occur in the photocathode compartment using $(bpy)Os(das)_2^{2+}$ as the chromophore. Excited state lifetimes, emission quenching and conventional flash photolysis experiments were undertaken in order to obtain rate constants and to verify the existence of the several steps expected to play a role in the photoelectrochemical mechanism. Using the experimental conditions of the cells, the excited state lifetimes in deaerated and air-saturated solution respectively are $\tau^0 = 1640$ ns and $\tau = 555$ ns. The shortened lifetime in the presence of O_2 is an expected result since O_2 is known to quench $Ru(bpy)_3^{2+*}$ and related excited states by energy transfer giving $O_2(^1\Delta_g)$ [26].

The rate constant for excited state quenching by NAr_3

$$(bpy)Os(das)_2^{2+*} + NAr_3 \xrightarrow[k_q]{} (bpy)Os(das)_2^{+} + NAr_3^{+} \quad (21)$$

in deaerated acetonitrile obtained using the Stern–Volmer technique is $k_q = (2.00 \pm 0.03) \times 10^8$ M^{-1} s^{-1} [27]. An important point to emerge from the quenching study was the fact that the cell efficiencies cited in Table 1 are severely limited in some cases by the limited solubility of the quencher in the medium, 7×10^{-3} M. Even in a solution saturated in quencher, the per cent quenching is only 72%. As noted above, the efficiency values ϕ'_{cell} cited in Table 1 are for solutions saturated in quencher.

The rate constant for back electron transfer or "recombination"

$$(bpy)Os(das)_2^{+} + NAr_3^{+} \xrightarrow[k_b]{} (bpy)Os(das)_2^{2+} + NAr_3 \quad (22)$$

as determined by conventional flash photolysis is $k_b = 2.0 \times 10^9$ M^{-1} s^{-1}.

Before a complete kinetic scheme can be constructed, the fact that ϕ'_{cell} can exceed unity, as shown by the value for $Ru(4,4'\text{-}(CO_2Et)_2bpy)_3^{2+}$ in Table 1, must also be taken into account. From the earlier work based on photochemically generated $Ru(bpy)_3^{+}$, reduction of O_2 by $(bpy)Os(das)_2^{+}$ is expected to be rapid [23]:

$$(bpy)Os(das)_2^{+} + O_2 \longrightarrow (bpy)Os(das)_2^{2+} + O_2^{-} \quad (23)$$

and followed by rapid protonation

$$O_2^{-} + H^{+} \longrightarrow HO_2 \quad (24)$$

in acidic acetonitrile. The most straightforward explanation of quantum yields approaching 2 is that reductive capture of HO_2 by a second molecule of NAr_3 must occur

$$HO_2 + NAr_3 + H^{+} \longrightarrow H_2O_2 + NAr_3^{+} \quad (25)$$

which would lead to a doubling in the amount of oxidative carrier NAr_3^{+}. Capture by NAr_3^{+} is in competition with disproportionation

$$2HO_2 \longrightarrow H_2O_2 + O_2 \quad (14)$$

If disproportionation were the dominant pathway for the conversion of HO_2 into H_2O_2, the limiting value for ϕ'_{cell} would be unity.

With the available experimental evidence in hand, it is possible to propose the series of reactions in Fig. 6 to explain the operation of the excited state half-cell based on $(bpy)Os(das)_2^{2+}$ as the chromophore. In the figure, reactions which compete with the appearance of the photoproducts H_2O_2 and NAr_3^{+} are blocked off in square brackets. Reactions which were not observed directly but appear to be demanded by earlier observations and/or are required by our results are blocked off by braces. When added up, the reactions in Fig. 6 predict a maximum per photon absorbed quantum yield of 2, but only if disproportionation of HO_2 is negligible.

3.5. Quantum yield variations

In order to test further the pattern of reactions proposed in Fig. 6 and to obtain quantitative insight into the operation of the cell, a series of photocharge measurements was undertaken in which the concentrations of the various components were varied. Equation (19) provides a quantitative basis for relating the photocharge response of the cell to the mechanism in Fig. 6 once an expression for ϕ_{cell} has been derived. ϕ_{cell} dictates the cell response past the light absorption step in Fig. 6 and is itself dictated by the series of subsequent chemical steps.

From the proposed mechanism in Fig. 6, ϕ_{cell} can be written as the product of the efficiencies of three separate steps and a numerical factor of 2 as shown the equation

$$\phi_{cell} = 2\phi_q\phi_{sep}\phi_{capture} \quad (26)$$

$$(bpy)Os(das)_2^{2+} \xrightarrow{h\nu} (bpy)Os(das)_2^{2+*}: I^0(1 - 10^{-A_{Os}}) \frac{A_{Os}}{A_{Os} + A_{NAr_3^+}}$$

$$\left[\begin{array}{l} (bpy)Os(das)_2^{2+*} \longrightarrow (bpy)Os(das)_2^{2+}: 1/\tau^0 \\ (bpy)Os(das)_2^{2+*} + O_2 \longrightarrow (bpy)Os(das)_2^{2+} + {}^1O_2: k_{O_2} \end{array} \right]$$

$$(bpy)Os(das)_2^{2+*} + NAr_3 \longrightarrow (bpy)Os(das)_2^{+} + NAr_3^{+}: k_q\phi_{sep}$$

$$[(bpy)Os(das)_2^{+} + NAr_3^{+} \longrightarrow (bpy)Os(das)_2^{2+} + NAr_3: k_b]$$

$$(bpy)Os(das)_2^{+} + O_2 \longrightarrow (bpy)Os(das)_2^{2+} + O_2^{-}: k'_{O_2}$$

$$\left\{ \begin{array}{l} O_2^- + H^+ \longrightarrow HO_2 \\ 2HO_2 \longrightarrow H_2O_2 + O_2 \\ HO_2 + NAr_3 \longrightarrow HO_2^- + NAr_3^+ \\ HO_2^- + H^+ \longrightarrow H_2O_2 \end{array} \right\}$$

Net reaction: $O_2 + 2H^+ + 2NAr_3 + h\nu \longrightarrow H_2O_2 + 2NAr_3^+$
Electrode reaction: $2NAr_3^+ + 2e^- \longrightarrow 2NAr_3$

Fig. 6. Scheme of the operation of the excited state half-cell based on $(bpy)Os(das)_2^{2+}$.

The terms in the order in which they appear in eqn. (26) are defined as follows.

(1) The factor of 2 arises from the apparent doubling in NAr_3^+ as a consequence of capture of HO_2 by NAr_3 (reaction (25)).

(2) In terms of the rate constants in Fig. 6, the quenching efficiency ϕ_q is given by

$$\phi_q = \frac{k_q[NAr_3]}{1/\tau^0 + k_q[NAr_3] + k_{O_2}[O_2]} \tag{27}$$

Defining the rate constant for excited state decay in an air-saturated solution as $1/\tau$ and that in a deoxygenated solution as $1/\tau^0$

$$\frac{1}{\tau} = \frac{1}{\tau^0} + k_{O_2}[O_2] \tag{28}$$

the quenching efficiency is given by

$$\phi_q = \frac{k_q[NAr_3]}{1/\tau + k_q[NAr_3]} \tag{29}$$

Equation (28) includes contributions to excited state decay both from the intrinsic radiative and non-radiative decay processes of the excited state ($1/\tau^0$) and from energy transfer quenching by O_2 ($k_{O_2}[O_2]$). Variations in the quenching efficiency probably account for a significant part of the variations in ϕ'_{cell} with chromophore in Table 1. The relatively small values for the bpym and bpyz quenchers are a direct consequence of shortened excited state lifetimes. The lifetime of $Ru(bpyz)_3^{2+*}$ under actual cell conditions in acidified acetonitrile is far less than cited in Table 1 because protonation at a ligand leads to a significant decrease in lifetime [28].

(3) The separation efficiency ϕ_{sep} is the efficiency with which the separated redox products appear in solution following electron transfer quenching. The series of reactions which lead to quenching and separated redox products are shown in Fig. 7. Figure 7 is based on an earlier scheme given by Rehm and Weller for the fluorescence quenching of a series of aromatic excited states [29] and has provided a basis for the estimation of excited state redox potentials [30, 31]. Past the quenching step, the appearance of separated redox products (k_3) is in competition with back electron transfer (k_4) before separation can occur. In terms of the rate constants of Fig. 7, ϕ_{sep} is given by

$$\phi_{sep} = \frac{k_3}{k_3 + k_4} \tag{30}$$

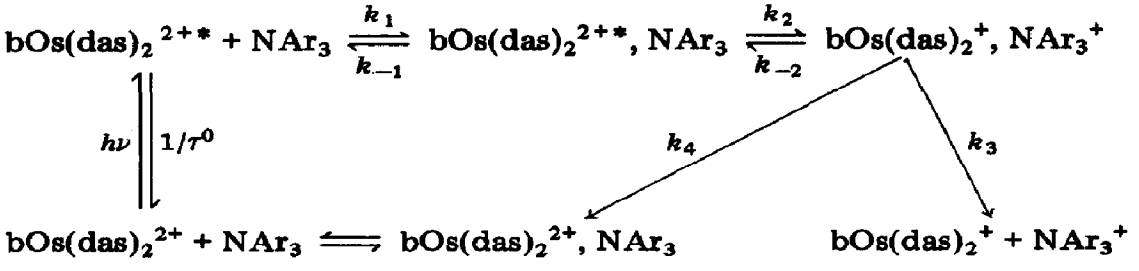

b ≡ 2,2′-bipyridine

Fig. 7. Series of reactions which lead to quenching and separated redox products.

(4) Capture of $(bpy)Os(das)_2^+$ by O_2 to give O_2^- and ultimately H_2O_2 is in competition with back electron transfer with NAr_3^+ to give back $(bpy)Os(das)_2^{2+}$ and NAr_3. The O_2 capture efficiency $\phi_{capture}$ predicted by Fig. 6 is given by

$$\phi_{capture} = \frac{k'_{O_2}[O_2]}{k'_{O_2}[O_2] + k_b[NAr_3^+]} \tag{31}$$

As noted below, under the conditions used to test the form of eqn. (31), $\phi_{capture} = 1$ except in solutions very dilute in O_2.

In eqns. (26) - (31) there are clear predictions as to how ϕ_{cell} and, through ϕ_{cell}, q_p are expected to vary with the concentrations of the various components. A series of experiments was carried out to test the predictions using the experimental conditions cited in appropriate figure captions. The results are summarized below.

(1) Quencher. The dependence of the cell response on quencher concentration is predicted to take the form shown in

$$\frac{1}{q_p} = \frac{1}{2M\phi_{sep}} \frac{1}{\tau k_q} \frac{1}{[NAr_3]} + \frac{1}{2M\phi_{sep}} \tag{32}$$

which follows from eqns. (19), (26) and (27), on the assumption that $\phi_{capture} = 1$. At a constant photolysis time the quantity M is a cell constant given by

$$M = nFI^0(1 - 10^{-A_{Os}}) \frac{A_{Os}}{A_{Os} + A_{NAr_3^+}} t \tag{33}$$

A plot of $1/q_p$ *versus* $1/[NAr_3]$ is shown in Fig. 8 from which the predicted linear relationship between $1/q_p$ and $1/[NAr_3]$ is, in fact, observed. Experimental data could only be taken to the solubility limit of NAr_3 in the medium (7×10^{-3} M).

From the intercept of the plot in Fig. 8 (6.3 ± 1.8 C^{-1}), $\phi_{sep} = 0.79 \pm 0.24$ under conditions where $M = 0.101$ and A_{Os}(436 nm) = 0.090. In a related photoelectrochemical experiment $\phi_{sep} = 0.84 \pm 0.14$ was found for the quenching of $Ru(bpy)_3^{2+*}$ by $Co(NH_3)_5Cl^{2+}$ in water [25]. ϕ_{sep} values approaching unity have also been determined for the quenching of $Ru(bpy)_3^{2+*}$ by organic amines in dimethylformamide [32] and by substituted

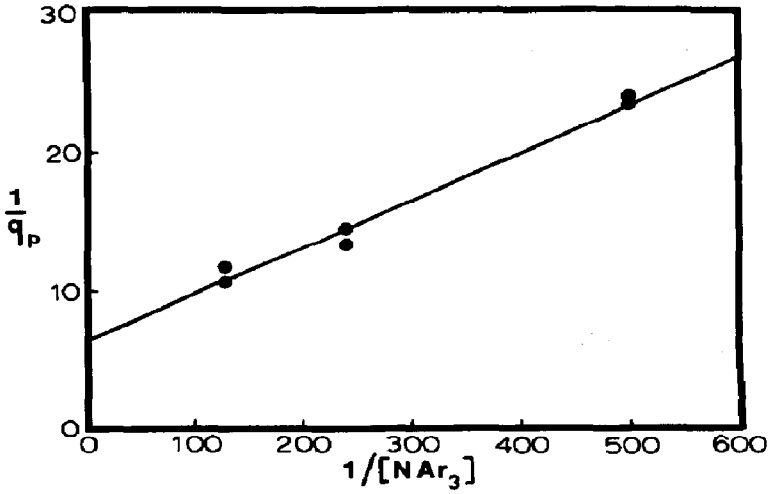

Fig. 8. Plot of $1/q_p$ (C^{-1}) *vs.* $1/[NAr_3]$ under the same conditions as in Fig. 4 except with varying amounts of NAr_3 (slope, 0.034 ± 0.005 M C^{-1}; correlation coefficient, 0.993). Using the intercept 6.3 ± 1.8 C^{-1}, $\phi_{sep} = 0.79 \pm 0.12$ based on eqn. (32) with $M = 0.101$.

phenolate anions in water at elevated temperatures or in ethanol–water or acetone–water mixtures rich in the organic solvent [33].

(2) Acid. Although an acid dependence is not included explicitly in the quantum yield expression, the addition of acid is essential for the net conversion of O_2 to H_2O_2. The experimentally determined variations in q_p with $[HClO_4]$ in Table 2 point to three important facts. (1) Even at 0.7 M added acid the cell operates efficiently, showing that the quencher is not significantly protonated. (2) The cell efficiency is relatively independent of $[HClO_4]$ over a broad range of concentrations. (3) Some acid must be added, as required by the net reaction. A kinetic basis for the proton requirement is that O_2^- is relatively stable in dry organic solvents [34 - 36] and if not removed by protonation can undergo back electron transfer with NAr_3^+:

$$NAr_3^+ + O_2^- \longrightarrow NAr_3 + O_2 \qquad (34)$$

TABLE 2

Dependence of q_p on added $[HClO_4]$[a]

$[HClO_4]$ (M)	q_p [b]
7×10^{-1}	0.079
1.2×10^{-1}	0.096, 0.092
1.2×10^{-2}	0.090, 0.083
2.4×10^{-3}	0.083, 0.078
2.4×10^{-4}	0.047, 0.046
0	0.002, 0.002

[a]Conditions as in Fig. 4 except with the amount of added $HClO_4$ varied.
[b]The results of duplicate determinations are listed.

(3) Oxygen. The dual role of O_2 as a competitive quencher for the excited state and as a necessary scavenger for $(bpy)Os(das)_2^+$ has already been introduced. In the presence of high concentrations of O_2 it follows from eqn. (31) that $\phi_{capture} \rightarrow 1$. When $\phi_{capture} = 1$, $1/q_p$ is predicted to vary linearly with $[O_2]$ as shown in

$$\frac{1}{q_p} = \frac{1}{2M\phi_{sep}} \frac{k_{O_2}[O_2]}{k_q[NAr_3]} + \frac{1}{2M\phi_{sep}}\left(1 + \frac{1}{k_q\tau^0[NAr_3]}\right) \qquad (35)$$

which follows from eqns. (19), (26) and (27).

At "high" partial pressures of O_2, $1/q_p$ does vary linearly with $[O_2]$, as shown in Fig. 9. The plot in Fig. 9 is shown in terms of partial pressure of O_2 (in atmospheres) obtained using O_2–N_2 mixtures, rather than concentration, because the Henry's law constant for O_2 under our conditions is not known. For this reason, the slope of Fig. 9 cannot be used to calculate ϕ_{sep}, even though a value of $k_{O_2}[O_2] = 1.19 \times 10^6$ s^{-1} can be calculated from

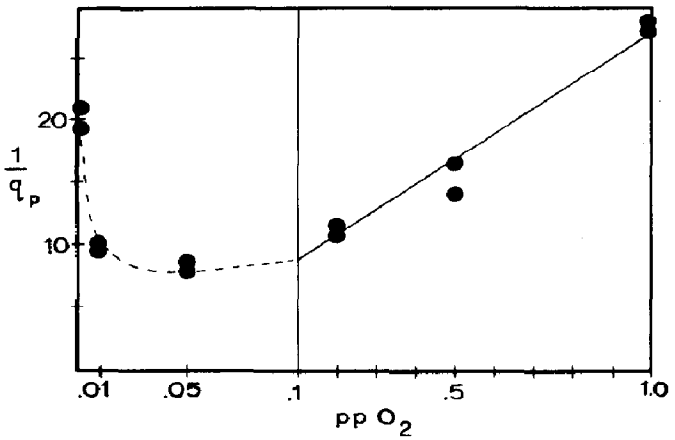

Fig. 9. Plot of $1/q_p$ (C^{-1}) *vs.* partial pressure of O_2 (atm) using the conditions of Fig. 4 except varying the partial pressure of O_2 using O_2–N_2 gas mixtures. For the linear region, in the $1/q_p$ *vs.* partial pressure O_2 plot (partial pressure O_2, 0.05), slope, 20 ± 3 C^{-1} atm^{-1}; intercept, 6.7 ± 1.8 C^{-1}; correlation coefficient, 0.988. The change in scale at 0.1 partial pressure O_2 should be noted.

lifetimes in aerated and deaerated solution using the Stern–Volmer relationship. However, extrapolating Fig. 9 to zero concentration and using the experimental values of $M = 0.101$ ($[NAr_3] = 7 \times 10^{-3}$ M) the independently measured values of $k_q = 2.0 \times 10^8$ M^{-1} s^{-1} (from a Stern–Volmer experiment) and $\tau^0 = 1580$ ns (in deaerated solution) [27], and the experimental intercept = 6.7 ± 1.8 C^{-1}, eqn. (35) gives $\phi_{sep} = 1.07 \pm 0.20$. ϕ_{sep} values of greater than unity are obviously not possible. However, given the experimental uncertainties involved, the estimate obtained for ϕ_{sep} does suggest that the separated redox products do indeed appear with a high efficiency following quenching.

The efficiency of the cell initially increases as the partial pressure of O_2 decreases because energy transfer quenching by O_2 becomes less important. From the plot in Fig. 9, a minimum is reached for partial pressures of O_2 between 0.01 and 0.05 which corresponds to a maximum in ϕ'_{cell} of 1.24 ± 0.07. At this point the magnitude of ϕ'_{cell} (eqn. (26)) is dictated by the product of $\phi_{sep} \approx 0.8 - 0.9$ and $\phi_q \approx k_q[NAr_3]/(1/\tau^0 + k_q[NAr_3]) \approx 0.72$. There is no longer a complication from energy transfer quenching by O_2 since $k_{O_2}[O_2] \ll (1/\tau^0 + k_q[NAr_3])$ in eqn. (27). However, at a partial pressure of O_2 below 0.05 the cell efficiency drops rapidly, presumably because the cell has entered the domain where $\phi_{capture}$ (eqn. (31)) becomes significantly less than unity. At this point, recombination between (bpy)Os(das)$_2^+$ and NAr_3^+ has become competitive with capture of (bpy)Os(das)$_2^+$ by O_2.

Some additional observations have been made which give insight into the operation of the photoelectrode.

(1) Long-term photolysis. The results of a series of long-term photolyses showed that photocurrents decreased less than 5% after 4 h which

typically corresponded to about 27 turnovers per metal complex sensitizer. After 12 h, photocurrents remained fairly constant, but extensive diffusion of the osmium(II) complex into the middle compartment had occurred. After a 12 h photolysis period the dark (baseline) current had drifted about 30% from the initial value before photolysis was initiated.

(2) Added H_2O_2. H_2O_2 is the net photoproduct in the cathode compartment. Given the series of redox steps in Fig. 6, it is conceivable that H_2O_2 could also act as an interfering scavenger by acting either as a reductant toward NAr_3^+ or as an oxidant toward $(bpy)Os(das)_2^+$. To put the concentrations involved into perspective, after 20 min of photolysis under our conditions, about 5×10^{-5} M H_2O_2 is produced. In experiments where H_2O_2 was added to the photocathode prior to photolysis, there was no significant effect on the observed steady state photocurrent for concentrations of added H_2O_2 up to 6×10^{-3} M.

4. Conclusions

We have described here the design and operation of a series of oxidative excited state photoelectrodes in which H_2O_2 and $N(p\text{-}C_6H_4Br)_3^+$ are produced in a single-cell compartment with a per photon absorbed quantum efficiency that can approach 2. The photoelectrode provides a basis for carrying out an oxidation in a second cell compartment and, in our experiments, provided a basis for the net excited state photoelectrochemical cell

$$2H^+ + O_2 + 2Br^- \xrightarrow{h\nu} H_2O_2 + Br_2 \qquad (7)$$

The design of the electrode was based on the series of one-electron transfer events summarized in Fig. 6. The properties of the cell are consistent with the pattern of reactions in the scheme including the successful prediction of the dependence of ϕ'_{cell} on the incident light intensity, the quencher, sensitizer and O_2 concentrations, as well as successfully predicting a limiting value of $\phi'_{cell} = 2$.

Our ability to design the H_2O_2–Br_2 photoelectrochemical cell arose from a combination of properly interwoven factors.

(1) There is a critical chain of three redox events involving four redox couples

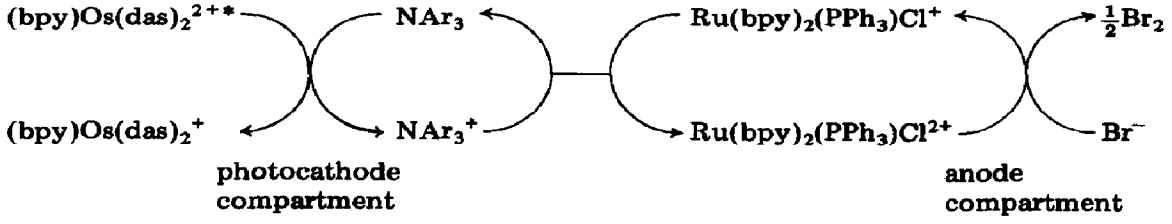

including the electron transfer catalyst $Ru(bpy)_2(PPh_3)Cl^{2+/+}$. For the chain of redox events to occur spontaneously, the order of decreasing potentials must be $E^{0\prime}(Os^{2+*/+}) > E^{0\prime}(NAr_3^{+/0}) > E^{0\prime}(Ru^{III/II}) > E^{0\prime}(Br_2/Br^-)$.

(2) O_2 plays a dual role both as the basis for H_2O_2 production by scavenging $(bpy)Os(das)_2^+$ before recombination can occur and as a debilitating component because of energy transfer quenching. It is essential that high concentrations of reductive quencher are used so that reductive quenching can compete with energy transfer to O_2.

(3) The successful operation of the cell relies on favorable relative rates for a number of one-electron transfer processes as summarized in Fig. 6. Using different cell conditions or changing the redox potential characteristics of the quencher couple could significantly affect the output of the cell.

(4) In this type of application it is obviously important that at least one of the two product couples, H_2O_2/O_2 and Br_2/Br^-, is irreversible electrochemically or that their back reaction, $Br_2 + H_2O_2 \rightarrow 2Br^- + 2H^+ + O_2$, is non-spontaneous in order to avoid back electron transfer from occurring indirectly through the electrochemical cell.

Although the cell design used here is relatively primitive and further experiments are needed to test the feasibility of large-scale chemical production in a variety of solvents, the potential significance of our observations should not be overlooked. From a general point of view, an apparatus is now available for delivering photochemically derived oxidative equivalents at an anode at relatively oxidizing potentials (1.07 V(SSCE)) with concomitant production of H_2O_2 in the photocathode compartment. This is a significantly high potential, sufficient thermodynamically to drive an extensive range of inorganic and organic oxidations including the epoxidation of olefins and the oxidative activation of any hydrocarbon.

Acknowledgment

Acknowledgment is made to the U.S. Department of Energy under Grant DE-AS05-78ER06034 for support of this research.

References

1 K. Kalyanasundaram and M. Grätzel, *Angew. Chem., Int. Edn. Engl., 18* (1979) 701.
2 C.-T. Lin and N. Sutin, *J. Phys. Chem., 80* (1976) 97.
3 T. L. Osif, N. N. Lichtin and M. Z. Hoffman, *J. Phys. Chem., 82* (1978) 1778.
4 P. J. DeLaive, B. P. Sullivan, T. J. Meyer and D. G. Whitten, *J. Am. Chem. Soc., 101* (1979) 4007.
5 S. O. Kobayashi, N. Furuta and O. Simamura, *Chem. Lett.*, (1976) 503.
6 M. Neumann-Spallart, K. Kalyanasundaram, C. Grätzel and M. Grätzel, *Helv. Chim. Acta, 63* (1980) 1111.
7 B. Durham and T. J. Meyer, *J. Am. Chem. Soc., 100* (1978) 6286.

8 B. Durham, W. J. Dressick and T. J. Meyer, *J. Chem. Soc., Chem. Commun.*, (1979) 381.
9 D. P. Rillema, W. J. Dressick and T. J. Meyer, *J. Chem. Soc., Chem. Commun.*, (1980) 247.
10 M. Neumann-Spallart and K. Kalyanasundaram, *J. Phys. Chem., 86* (1982) 2681.
11 W. J. Dressick, T. J. Meyer, B. Durham and D. P. Rillema, *Inorg. Chem., 21* (1982) 3451.
12 G. A. Neyhart, J. L. Marshall, W. J. Dressick, B. P. Sullivan, P. A. Watkins and T. J. Meyer, *J. Chem. Soc., Chem. Commun.*, (1982) 915.
13 T. N. Baker, W. P. Doherty, W. S. Kelley, W. Newmeyer, J. E. Rogers, R. E. Spalding and R. I. Walter, *J. Org. Chem., 30* (1965) 3714.
14 J. V. Caspar, *Ph.D. Dissertation*, University of North Carolina, Chapel Hill, NC, 1982.
15 D. A. Buckingham, F. P. Dwyer, H. A. Goodwin and A. M. Sargeson, *Aust. J. Chem., 17* (1964) 315.
16 D. P. Rillema, G. Allen, T. J. Meyer and D. Conrad, *Inorg. Chem., 22* (1983) 1617.
17 P. J. DeLaive, T. K. Foreman, C. Giannotti and D. G. Whitten, *J. Am. Chem. Soc., 102* (1980) 5627.
18 B. P. Sullivan, D. J. Salmon and T. J. Meyer, *Inorg. Chem., 17* (1978) 3334.
19 J. G. Calvert and J. N. Pitts, *Photochemistry*, Wiley, New York, 1966, p. 783.
20 B. Durham, J. V. Caspar, J. K. Nagle and T. J. Meyer, *J. Am. Chem. Soc., 104* (1982) 4803.
21 A. I. Popov and D. H. Geske, *J. Am. Chem. Soc., 80* (1958) 5346.
22 H. A. Mottola, B. E. Simpson and G. Gorin, *Anal. Chem., 42* (1970) 410.
23 C. P. Anderson, D. J. Salmon, T. J. Meyer, and R. C. Young, *J. Am. Chem. Soc., 99* (1977) 1980.
24 B. H. J. Bielski, *Photochem. Photobiol., 28* (1978) 645.
25 W. J. Dressick, T. J. Meyer and B. Durham, *Isr. J. Chem., 22* (1982) 153.
26 J. N. Demas, E. W. Harris and R. P. McBride, *J. Am. Chem. Soc., 99* (1977) 3547.
27 W. J. Dressick, *Ph.D. Dissertation*, University of North Carolina, Chapel Hill, NC, 1981.
28 R. J. Crutchley, N. Kress and A. P. B. Lever, *J. Am. Chem. Soc., 105* (1983) 1170.
29 D. Rehm and A. Weller, *Ber. Bunsenges. Phys. Chem., 73* (1969) 834; *Isr. J. Chem., 8* (1970) 259.
30 C. R. Bock, J. A. Connor, A. R. Gutierrez, T. J. Meyer, D. G. Whitten, B. P. Sullivan and J. K. Nagle, *J. Am. Chem. Soc., 101* (1979) 4815
31 C. R. Bock, T. J. Meyer and D. G. Whitten, *J. Am. Chem. Soc., 97* (1975) 2909.
32 H. Shioyama, H. Masuhara and N. Mataga, *Chem. Phys. Lett., 88* (1982) 161.
33 K. Miedlar and P. K. Das, *J. Am. Chem. Soc., 104* (1982) 7462.
34 D. L. Maricle and W. G. Hodgson, *Anal. Chem., 37* (1965) 1562.
35 D. T. Sawyer and J. L. Roberts, *J. Electroanal. Chem. Interfacial Electrochem., 12* (1966) 90.
36 R. Dietz, A. E. J. Forno, B. E. Larcombe and M. E. Peover, *J. Chem. Soc. B*, (1970) 816.